Scanning Force Microscopy

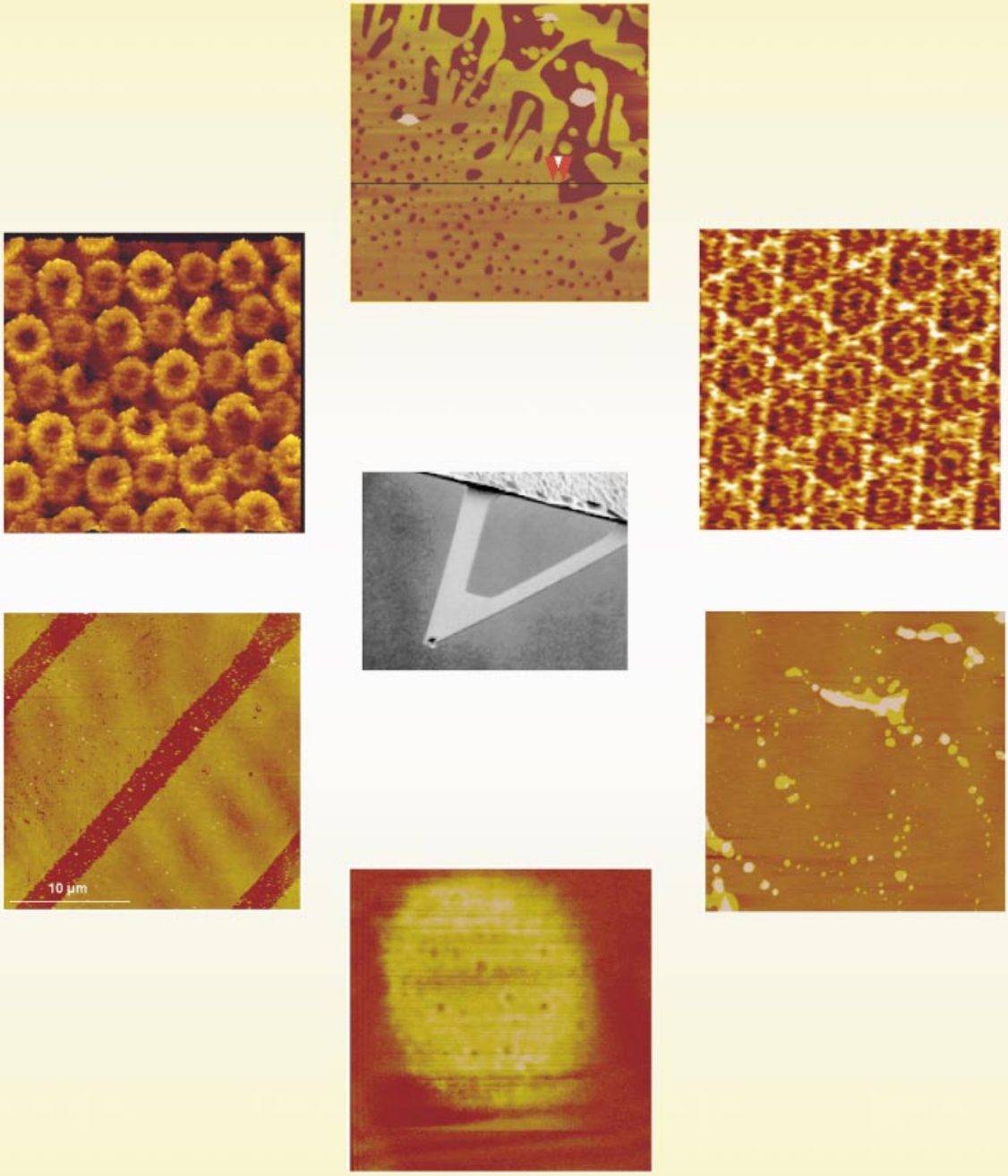

# of Solid-Supported Membranes

  1439-4227/01/02/11 $ 17.50+.50/0 CHEMBIOCHEM **2001**, 2, 798 – 808

Scanning Force Microscopy of Artificial Membranes

Andreas Janshoff[b] and Claudia Steinem*[a]

Visualization of biological membranes by scanning force microscopy (SFM) has tremendously improved the current understanding of protein – lipid interactions under physiological conditions. SFM is the only tool to directly image processes on surfaces in aqueous solution at molecular resolution. Besides being a supportive means to confirm results on lipid phases and domains obtained from fluorescence spectroscopy, calorimetry, and X-ray crystallography, SFM has contributed distinct aspects on the formation of 2D crystals of various membrane-confined proteins and morphological changes of membranes due to the interaction of peptides and proteins. This review will focus on recent results in SFM imaging of artificial solid-supported membranes, their phase behavior as a response to the environment, and changes in membrane morphology induced by the partitioning of peptides and proteins.

KEYWORDS:

biosensors · membrane proteins · membranes · phospholipids · scanning probe microscopy

1. Introduction

Phospholipid bilayers form the basic framework of biological membranes. Membrane phospholipids are not only the passive structural matrix, but play an active role in signal transduction and functional modulation and house a large number of membrane proteins such as channels, ion pumps, and receptor proteins, which regulate various cellular and subcellular functions and activities. To understand the properties of biological membranes, it is of great importance to study the structural organization of lipids and membrane proteins as well as their interplay. Since the invention of the scanning force microscope operating in an aqueous environment,[1] this technique has evolved as a routine tool for imaging biological samples and was proven to be ideally suited for studying lipid bilayers immobilized on atomically flat surfaces such as mica in an aqueous environment. The general setup of a common scanning force microscope is illustrated in Figure 1 A.

In principle, there are two main techniques to prepare solid-supported lipid bilayers on mica or glass surfaces: (i) vesicle spreading (Figure 1 B)[2] and (ii) Langmuir – Blodgett transfer of lipid layers.[3, 4] Both techniques can lead to almost defect-free lipid bilayers that are easy to image by scanning force microscopy (SFM). In Figure 1 C, an SFM image of a lipid bilayer obtained by vesicle fusion on mica is depicted. An area with a large number of defects is shown allowing one to distinguish between membrane-covered areas (bright areas) and uncovered mica areas (darker areas). By measuring the height difference between the membrane and the mica surface an accurate value for the membrane thickness can be obtained.

Besides membrane topography, SFM of lipid membranes offers the advantage of delivering spatially resolved information about material properties such as viscoelasticity, friction, adhesion, and surface charges. The detection of these membrane properties has led to a more visual understanding of basic membrane processes comprising issues of phase separation, membrane – peptide interactions, and the impact of membrane-active compounds on the integrity of lipid bilayers. Moreover, owing to the flat appearance of a lipid layer on mica surfaces, high-resolution images of lipids and proteins can be obtained by SFM.

This review will give an overview of the recent advances that have been achieved in studying lipid bilayers and membrane proteins as well as the interaction of proteins and peptides with solid-supported bilayers through the use of SFM. In the last chapter (Section 5), the application of laterally patterned lipid membranes used for biosensing will be discussed. By means of SFM these patterned membranes can be visualized and protein adsorption can be monitored in situ.

2. Lipid bilayer structures

The fluid mosaic model has been the framework for our understanding of biological membranes for more than two decades.[5] It is viewed as a heterogeneous system that is organized into lipid and proteinacious domains. SFM is ideally suited for studying the lateral organization of lipid bilayers under physiological conditions without specimen treatment. Lipid

[a] *Prof. Dr. C. Steinem*
Institut für Analytische Chemie, Chemo- und Biosensorik
Universität Regensburg
93040 Regensburg (Germany)
Fax: (+ 49) 941-943-4491
E-mail: claudia.steinem@chemie.uni-regensburg.de

[b] *Prof. Dr. A. Janshoff*
Institut für Physikalische Chemie
Johannes-Gutenberg-Universität
Jakob-Welder-Weg 11, 55128 Mainz (Germany)

domains in binary mixtures were visualized by SFM, making use of topography differences between the distinct domains.[4, 6–12] Even if there were no height difference between the lipid domains, differences in adhesion or viscoelasticity may account for contrast between the two kinds of domains.[7, 13–15] For instance, Lee and co-workers thoroughly investigated mixed monolayers of 1,2-distearoyl-*sn*-glycero-3-phosphoethanolamine (DSPE)/1,2-dioleoyl-*sn*-glycero-3-phosphoethanolamine (DOPE) and monogalactosyldiglyceride (MGDG)/DOPE by SFM.[7, 13, 14] They found a direct correlation between the topographic contrast and the load applied by the SFM tip. DSPE/DOPE and MGDG/DOPE monolayers on a DSPE monolayer exhibit a significant height difference at loads lower than the breakthrough force[16] of each type of domain and low topographic contrast at loads above the breakthrough force of both lipid domains. With respect to lipid domains, Ca^{2+}-induced phase separation is of particular interest, since it is thought to play an essential role in membrane fusion and protein activity.[17] Shao and Yang investigated Ca^{2+}-induced domains in 1-palmitoyl-2-oleoyl-*sn*-glycero-3-phosphocholine (POPC)/1-palmitoyl-2-oleoyl-*sn*-glycero-3-phosphoglycerol (POPG) lipid bilayers and found a reduced height of approximately 1 nm for POPC domains in the presence of calcium ions.[12] Recently, Reviakine et al.[6] visualized the Ca^{2+}-dependent morphology of mixed 1,2-dipalmitoyl-*sn*-glycero-3-phosphocholine (DPPC)/1,2-dioleoyl-*sn*-glycero-3-phosphoserine (DOPS) and DPPC/1,2-dioleoyl-*sn*-glycero-3-phosphocholine (DOPC) bilayers by SFM. In the absence of Ca^{2+}, large, well-defined DPPC domains were found in both DPPC/DOPC and DPPC/DOPS bilayers, while in the presence of Ca^{2+} small isolated DPPC domains were found in DPPC/DOPS mixtures. Ca^{2+} had no effect on the organization of DPPC in

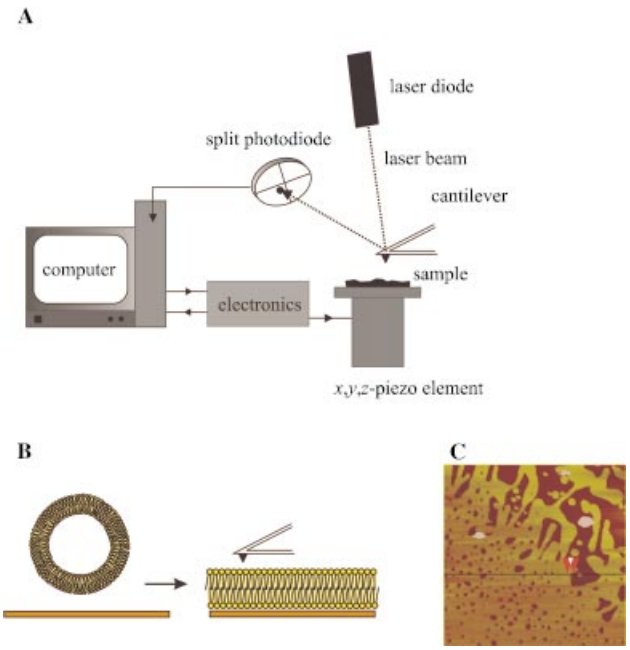

Figure 1. *A: Schematic drawing of a force microscope with a four-quadrant position-sensitive photo detector. The deflection of the cantilever is detected by the laser deflection reflected from the cantilever. The sample is positioned on a piezo element that is movable in three dimensions. The piezo element allows moving the sample in vertical dimension (z-piezo) and scanning the surface in the x,y plane (x,y-piezo). There are two different modes: In the constant-height mode, the cantilever deflection is detected without feedback control (applicable to very smooth surfaces), while in the constant-force mode the z-piezo compensates for possible cantilever deflections by changing the z position. B: Schematic drawing of vesicles spreading on a hydrophilic glass or mica surface forming planar bilayers. C: SFM image of a 1,2-dipalmitoyl-sn-glycero-3-phosphocholine (DPPC) bilayer on mica, obtained in contact mode. Image size is 5 × 5 μm^2. A region displaying large defects was chosen to obtain the thickness of the bilayer, which was 5.4 (± 0.2) nm.*

Andreas Janshoff,

born in 1966, studied biology and chemistry at the Westfälische Wilhelms Universität (WWU) in Münster (Germany), where he received his diploma in 1994. In 1997, he obtained his Ph.D. at the Institute for Biochemistry (WWU) under H.-J. Galla for studies on the biofunctionalization of gold surfaces and its applications in bioanalytics. As a postdoctoral fellow, he attended the group of M. Reza Ghadiri at the Scripps Research Institute, La Jolla, CA (USA), for 1½ years. During this time he worked on SFM imaging of lipid membranes. In 1999 he returned to the group of H.-J. Galla at the WWU to start his habilitation in close collaboration with the group of H. Fuchs at the Department of Physics (WWU). He was appointed to a professorship for physical chemistry at the Institute for Physical Chemistry of Johannes-Gutenberg-Universität in Mainz (Germany) in April 2001. His research fields include SFM of solid-supported lipid membranes, the development of new sensor systems based on micropatterned biofunctionalized surfaces, and the application of acoustic resonators as a tool to investigate adhesion and adsorption phenomena.

Claudia Steinem,

born in 1967, studied biology and chemistry at the Westfälische Wilhelms Universität (WWU) in Münster (Germany). Having obtained her Diploma in chemistry, she received her Ph.D. under H.-J. Galla for studies on the ion transport in solid-supported lipid bilayers in 1997. After a postdoctoral stay at the Scripps Research Institute in La Jolla, CA (USA), for 1½ years in the group of M. Reza Ghadiri, she returned as a Lise Meitner Fellow to the Institute for Biochemistry of the WWU in 1999. She finished her habilitation in February 2001 and was appointed to a professorship for bioanalytics at the Institute for Analytical Chemistry, Chemo- and Biosensors of the University of Regensburg (Germany). Her main research interests include the interactions of artificial peptides and annexins with lipid membranes and the development of new lipid membrane systems, based on composite structures, on porous surfaces.

DPPC/DOPC mixtures, and its effect was abolished by adding DOPC to DPPC/DOPS bilayers. Ross et al.[18] explored the calcium-induced formation of phosphatidylserine-enriched lipid domains in Langmuir – Blodgett (LB) monolayers composed of the binary mixture of the two saturated lipids DPPC and 1,2-dipalmitoyl-*sn*-glycero-3-phosphoserine (DPPS) in a molar ratio of 4:1 by means of SFM in combination with time-of-flight secondary-ion mass spectrometry (TOF-SIMS) and scanning electron microscopy. Domain formation only occurred in the presence of calcium ions. Since both lipids are in the gel state at room temperature and have the same acyl chain composition, differences in topography are marginal (0.03 nm). However, by means of lateral force microscopy, in which one measures the lateral forces exerted on the tip during imaging, lipid domains could be easily visualized (Figure 2). There are often conflicting results about Ca^{2+}-induced lipid domain formation, mainly arising from the fact that the occurrence of phase separation is indirectly concluded from the results. The major advantage of SFM is that it provides the most direct answer to the question of domain formation and simultaneously addresses domain size, form, and distribution in an aqueous environment.

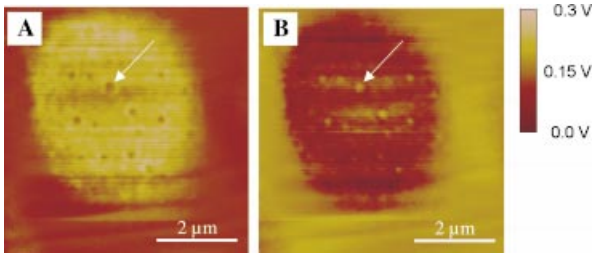

Figure 2. *Lateral force microscopy images of a lipid bilayer obtained in water. First, a DPPC monolayer was deposited onto mica at a surface pressure of 45 mN m^{-1} by Langmuir – Blodgett transfer followed by a second transfer of a DPPC/DPPS monolayer in a molar ratio of 4:1 at a surface pressure of 30 mN m^{-1} on water subphase. A: Forward scan, B: backward scan.[18]*

Besides domain formation in binary systems, it was shown by means of SFM that different lipid phases in neat systems could be visualized.[19, 20] It is known that short-chain alcohols and other amphiphiles such as anesthetics may induce interdigitated phases in gel-phase phosphatidylcholine (PC) bilayers by reducing the energy barrier that is due to entropic losses induced by the methyl group of the acyl chain pointing to the water phase. By fusing either DPPC or DSPC vesicles on mica, interdigitation induced by ethanol or propanol was visualized by SFM (Figure 3).[19] Interdigitation led to a height reduction of approximately 2 nm. Another interesting example is the observation of ripple phases by SFM.[21] A ripple phase—a phase in which the bilayer becomes wrinkled with a periodic modulation—occurring between the gel phase and the fluid phase has been described for PC bilayers. Mou et al.[22] used SFM to study ripple phases in supported 1,2-dimyristoyl-*sn*-glycero-3-phosphocholine (DMPC)/1,2-distearoyl-*sn*-glycero-3-phosphocholine (DSPC) bilayers. Surprisingly, they found that tris(hydroxymethyl)-aminomethane (Tris) induces ripple phases in supported dipentadecanol/PC bilayers, which generally do not form ripple phases at room temperature.

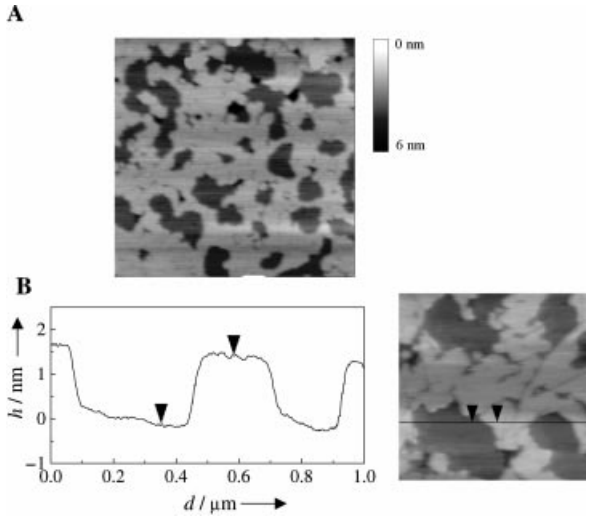

Figure 3. *A: SFM image (2.5 × 2.5 μm^2) of DPPC membranes spread on a mica surface after incubation in a 5% (v/v) ethanol solution obtained in 20 mM NaCl solution at room temperature. Ethanol-containing electrolyte was added to a preformed DPPC bilayer and the solid-supported membrane was incubated at 55 °C for 15 min in a closed SFM cell. B: The height difference between the two phases obtained from the average of 50 measurements is about (1.6 ± 0.2) nm.[60]*

3. Imaging of membrane-confined proteins

The applicability of SFM to imaging biological objects in a physiological environment has been demonstrated shortly after its invention. Though higher resolution images can be obtained by electron microscopy and X-ray crystallography, only SFM allows the direct imaging of proteins and their substructures in a native environment with a lateral resolution of 0.5 nm, which is particularly interesting with respect to membrane-confined proteins.

An easy and straightforward technique to image membrane-confined proteins is to form a lipid bilayer with an appropriate composition on an atomically flat surface and to add the peripheral membrane protein of interest to the buffer to allow for binding to the membrane. Recent work by Mueller et al.[23] and Janshoff et al.[24] demonstrated the feasibility of this technique to monitor the binding behavior of peripheral membrane proteins. Mueller et al.[23] were able to image the adsorption of myelin basic protein and cytochrome *c* to differently charged lipid bilayers. Myelin basic protein bound to acidic neutral and basic bilayers forming differently shaped protein domains, while cytochrome *c* only adsorbed to acidic bilayers forming characteristic ring-shaped aggregates. Janshoff et al.[24] investigated the binding of annexin I, a protein that belongs to a family of structurally related eukaryotic proteins, which reversibly bind membranes containing anionic phospholipids in a calcium-dependent manner. More than 160 different isoforms have been found in many organisms ranging from mammals to molds.[25] Annexin I is capable of aggregating and even fusing membrane vesicles.[26–29] However, the mechanism of membrane aggregation is still a matter of discussion. One question with respect to the association of annexin I with lipid bilayers is whether it binds in a monomeric fashion or as a dimer to

phospholipid bilayers and whether it solely binds to acidic phospholipids. To address this question, Janshoff et al.[24] utilized SFM on DPPC/DPPS Langmuir – Blodgett bilayers immobilized on mica to visualize annexin I binding. The addition of annexin I to an almost featureless bilayer results in the appearance of circularly shaped protein domains with an approximate size of 5 – 7 μm on top of the bilayer, exhibiting an average height of (3.2 ± 0.3) nm (Figure 4). The height indicates that annexin I binds in a monomeric fashion only to the DPPS-enriched domains. Crystallization of the protein as it was observed for annexin V on DOPC/DOPS membranes[6, 30–32] did not occur within the time of an experiment.

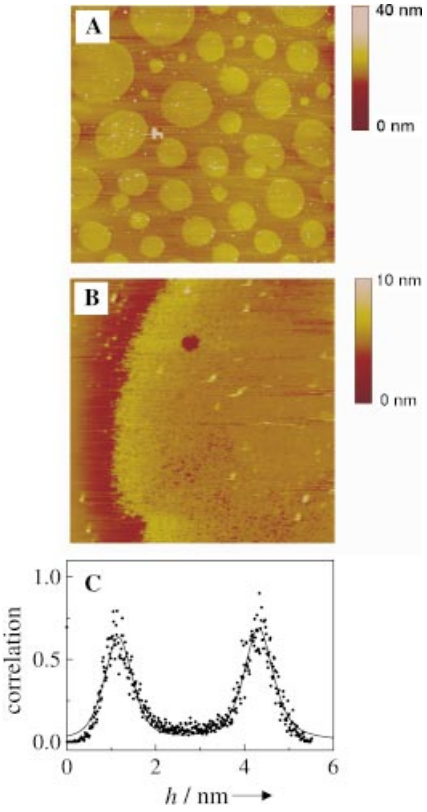

Figure 4. *A: SFM image (topography) of a Langmuir – Blodgett bilayer composed of DPPC as a first monolayer and a second DPPC/DPPS (4:1) monolayer deposited onto mica after addition of 1 μM annexin I in 50 mM Tris (pH 7.4) and 1 mM $CaCl_2$. The image size is 40 × 40 μm². B: Topographic image of a single lipid domain with adsorbed annexin I. Image size: 3 × 3 μm². C: Height analysis of a topographic image of annexin I domains adsorbed onto a DPPC/DPPS lipid layer. The histogram displays a Gaussian-filtered version of a depth analysis. Two well-separated height distributions attributed to the protein and the lipid layer, respectively, are decomposed by fitting mixed Lorentzian/Gaussian functions to the data shown as solid line. The height difference between the two peaks is 3.2 nm.[24]*

If membrane-associated proteins form two-dimensional (2D) crystals on the surface, SFM is capable of resolving single proteins with subnanometer resolution. With this technique Brisson and co-workers unraveled the molecular structure of annexin V on DOPC/DOPS lipid bilayers[6, 30–32] (Figure 5), while Mou et al.[33] reported on the successful imaging of cholera toxin B oligomers directly grown on ganglioside GM_1-containing (10 mol %) lipid bilayers varying in their lipid composition, including gel-phase lipids such as DPPC and fluid-phase lipids such as 1-palmitoyl-2-oleoyl-*sn*-glycero-3-phosphoethanolamine (POPE).

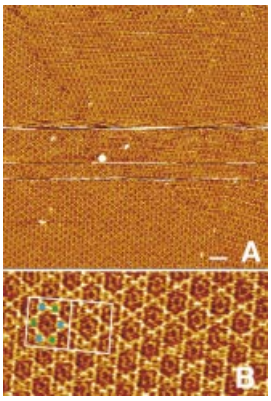

Figure 5. *SFM images of annexin V 2D crystals grown on DOPS-containing solid-supported membranes. A: Image size: 1.5 × 1.5 μm². B: Image size: 257 × 318 nm². The right part of the white box surrounds six annexin V trimers located at the vertices of a hexagon; a seventh trimer is located at the hexagon's center. In the left part of the box, the trimers are labeled with green and blue dots, respectively. The trimers labeled with a blue dot are rotated by 60° to the trimers labeled with a green dot. (The figure is courtesy of I. Reviakine and A. Brisson. Reprinted with permission from ref. [30]. Copyright 1998 Academic Press.)*

For integral membrane proteins, reconstitution into these artificial planar bilayers remains difficult. An interesting example is the reconstitution of a prepore of a staphylococcal α-hemolysin mutant in solid-supported egg PC bilayers on mica.[34] After formation of the bilayer, the purified protein was added to the bilayer for 5 – 12 days. By SFM the oligomeric state of the genetically engineered mutant in the lipid bilayer was resolved. More promising in most cases and mostly pursued to image membrane proteins is to use 2D protein crystals in order to get high-resolution images of these species and their arrangement in a lipid bilayer. Not only naturally occurring membrane fragments with a crystalline arrangement of membrane proteins are well suited, but also recrystallization of membrane proteins into well-ordered 2D crystals allows to obtain high-resolution images of these proteins. One prominent and extensively studied membrane protein is bacteriorhodopsin, a light-driven proton pump in the cell membrane of *Halobacterium salinarium*. Bacteriorhodopsin is densely packed in the so-called purple membrane forming a 2D trigonal lattice in the membrane. The protein is composed of seven closely packed transmembrane helices in which a retinal chromophore is embedded. By SFM, high-resolution images of the extracellular and cytoplasmic surface of purple membrane were obtained showing distinct features, which can be assigned to particular loops connecting the transmembrane helices.[35–41] Cleaving the Schiff base of bacteriorhodopsin leads to structural changes in the apoprotein. As observed by SFM, the bond cleavage results in a disassembly of the purple membrane crystal. SFM is not only an invaluable imaging technique, but also a nanoscopic actuator to manipulate single molecules as was demonstrated by combining SFM and single-molecule force spectroscopy. Oesterhelt et al.[42] were able to extract individual bacteriorhodopsin molecules helix by helix from the membrane by using an SFM tip. Upon extraction, the bacteriorhodopsin helices were found to unfold in an individual unfolding pathway. Bacteriorhodopsin is not the only example of high-resolution protein imaging. Hoh et al.[43] were able to image gap junction plaques purified from rat liver immobilized on glass supports, which is probably the first SFM work on a membrane protein

with convincing and reproducible images under nearly physiological conditions. Other examples include the nuclear pore,[44] the *Escherichia coli* water channel aquaporin Z,[45] porin OmpF from *E. coli*, hexagonally packed intermediate (HPI) layers from *Deinococcus radiodurans*,[40, 46, 47] and images of the photosystem I complex.[48] Recently, high-resolution images of subunit-III oligomers of chloroplast ATP synthase were obtained by Seelert et al.[49] (Figure 6).

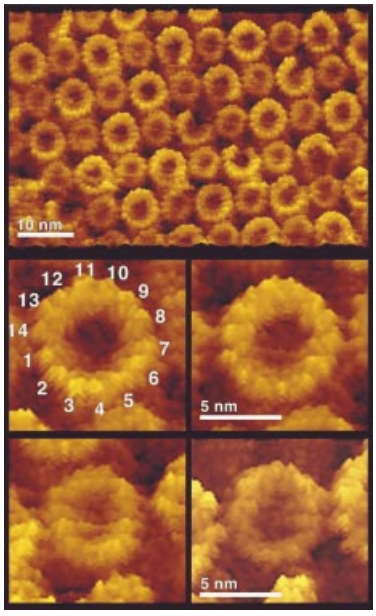

Figure 6. *SFM images of the subunit-III oligomers of chloroplast ATP synthase. Top: The distinct wide and narrow rings represent the two surfaces of the subunit-III oligomer; middle: close-up of the wide oligomer ends showing 14 subunits III; bottom: narrow oligomer ends. (The images are courtesy of D. J. Müller. Reprinted with permission from ref. [49]. Copyright 2000 Macmillan Magazines Ltd.)*

4. Interaction of peptides with membranes

The high lateral resolution of the scanning force microscope offers the possibility to probe the lateral segregation of peptides and lipids in biological membranes, which gives rise to different biological activities. The length scale of domains induced by peptides or other membrane-active compounds may be well below 100 nm and is therefore difficult to probe with other techniques such as fluorescence microscopy.

One of the first SFM studies on peptide-induced changes in membrane morphology was provided by Mou et al.[50] reporting on the aggregation of gramicidin A (gA) in supported gel-state phosphatidylcholine bilayers. Membrane formation was achieved by spreading mixed gA/DPPC vesicles on mica varying in the peptide-to-lipid ratio. Depending on the gA concentration, SFM images of those bilayers revealed gA-induced point-like and line-type aggregates with lateral dimensions of 3 – 4 nm. These aggregates appear as depressions, as expected from the difference in peptide length (gramicidin dimer (2.6 nm)) and bilayer thickness (4 – 5 nm). At higher gA concentrations (5 mol %), the membrane morphology went through a percolation-type transition in which most of the line-type aggregates have been interconnected, with point-like depressions still sustaining. Very high gA concentrations (10 mol %) resulted in complex bilayer morphology, albeit the planar character of the membrane still remained.

Recently, Rinia et al.[51] reported on the formation of striated domains induced by WALP peptides with the sequence acetyl-GWW(LA)$_n$WWA-ethanolamine ($n = 5$, 6, 8, 10) corresponding to the peptides WALP16, -19, -23, and -27. WALP peptides are model peptides exhibiting an alternate alanine – leucine stretch of variable length giving rise to a hydrophobic α helix flanked on both ends by tryptophan residues. WALP peptides have been successfully employed to study the effect of mismatch between the hydrophobic transmembrane regions of integral membrane proteins and the hydrophobic core of the lipid bilayers. In Figure 7, SFM images of striated domains induced by WALP23 in DPPC bilayers of different peptide concentrations are shown. At low WALP23 content, line-type depressions prevail along with the occurrence of point-like depressions and striated domains at the intersection of more than two line-type domains (Figure 7 A). The striated phase consists of low and high lines with a height difference of 0.3 nm. Increasing the amount of peptide is accompanied by a rising number of line-type depressions and striated domains in the bilayers (Figure 7 B). The structure is interpreted in terms of a deformed bilayer. The presence of the peptides perturbs the bilayer organization, resulting in a decrease in the tilt of the lipids between the peptide arrays. These lipids therefore appear as high lines. The striking similarity to the domain organization observed by Mou et al.[50] for gA in DPPC suggests that striated domains are formed directed by lipid rigidity or a general packing geometry.

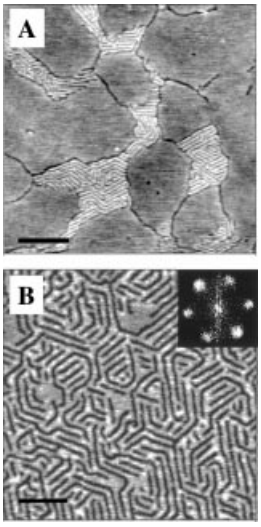

Figure 7. *Formation of striated domains induced by WALP23 in DPPC bilayers. A: SFM image of a DPPC bilayer containing 2 mol % WALP23. The image size is 500 × 500 nm^2, the scale bar 100 nm long. B: SFM image at high magnification of a striated domain, formed in a bilayer of DPPC with 10 mol % WALP23. The image size is 250 × 250 nm^2, with a scale bar length of 50 nm. The inset shows the 2D power spectrum of this domain, from which it is deduced that the average angle between the lines within the domains is 60° and their average distance 7.5 nm. (The images are courtesy of H. A. Rinia. Reprinted with permission from ref. [51]. Copyright 2000 American Chemical Society.)*

The impact of amphipathic peptides on membrane morphology has been demonstrated by SFM, illuminating the mode of action of melittin and a virus-derived peptide. Melittin, the major component of the bee venom of *Apis mellifera*, belongs to one of the best-studied amphipathic α-helical peptides.[52] It consists of 26 amino acids which are mainly hydrophobic, though it also contains six positive charges, four of which are located at the C terminus as Lys-Arg-Lys-Arg. Depending on conditions such as pH, ionic strength, and peptide

concentration, melittin is either monomeric or tends to form oligomers (tetramers) in solution. The enormous toxicity of melittin arises from its high membrane activity. Once bound to the cell surface, melittin induces lysis of the cell by forming defects in the lipid bilayer. It is still a matter of discussion whether membrane partition of melittin proceeds either by transmembrane-pore formation through a "barrel stave" mechanism or by membrane solubilization through a "carpet-like" mechanism (Figure 8 A).[53, 54] The "barrel stave" mechanism

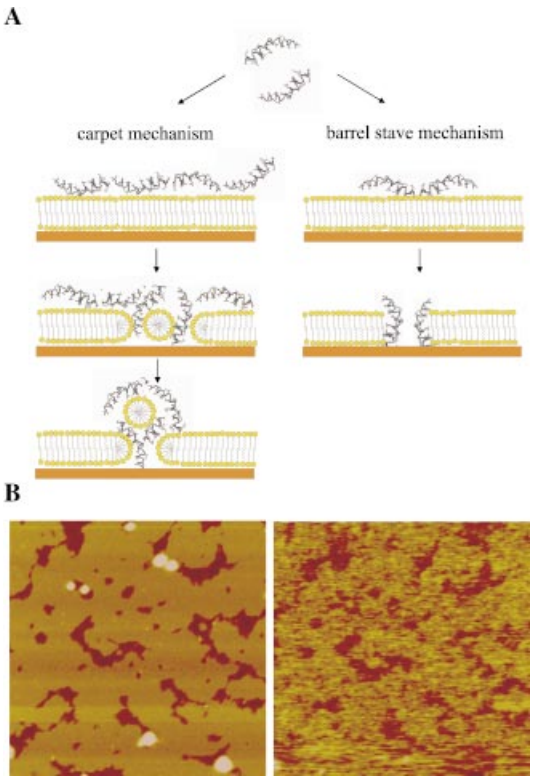

Figure 8. *A: Schematic representation illustrating the action of amphipathic membrane-active peptides on lipid membranes. B: SFM images (1.5 × 1.5 μm^2, height scale: 10 nm) obtained in tapping mode of POPC bilayers before (left image) and 5 min after (right image) addition of 2 μM melittin. The lipid structure is considerably altered, though the characteristic features in the figure on the left-hand side are still discernable after membrane disruption. The very high globular structures are vesicles attached to the lipid layer.*[56]

describes the formation of a transmembrane channel, in which the amphipathic helices form bundles with the hydrophobic residues pointing to the membrane interior and the hydrophilic side forming water-filled pores. Binding to the membrane is predominately driven by hydrophobic interactions with the lipid core. The "carpet-like" mechanism, however, describes the disruption of the membrane induced by an initial binding of the peptide, resulting in an orientation perpendicular to the surface normal and leading to a coverage resembling a carpet. After reaching a certain threshold concentration, the membrane can be permeated by dissolving small lipid aggregates covered by the peptide, thereby increasing its solubility. This mode of action is often accompanied by a change in lipid morphology from lamellar to non-lamellar phases.[55]

Supporting the vast amount of spectroscopic data, SFM was utilized to visualize for the first time morphological changes due to rupture of the lipid membrane and the formation of peptide–lipid aggregates or mixed micelles confirming a "carpet-like" mechanism.[56] To monitor the interaction of melittin/phospholipase A_2 with POPC membranes, an area with a significant number of defects—visible as darker areas—was chosen (Figure 8 B) and imaged several times in intermittent contact mode (tapping mode) to prove that no disruption of the POPC bilayer due to imaging occurs. Imaging of the membrane did not result in any morphological changes of the membrane. However, addition of a 2 μM melittin solution results in a fast and considerable change in membrane morphology. A lower, very soft lipid structure of approximately 2–3 nm height was observed, which started to dissolve. Due to the softness of the material, even tapping mode scanning manipulated the lipid structures. Imaging an area after addition of melittin and subsequent incubation for 10 min without imaging to prevent structural changes of the membrane leads to the observation of small globular structures with almost equal dimensions exhibiting a mean diameter of (100 ± 20) nm and a height of (18 ± 2) nm homogeneously distributed over the entire area. Steinem et al.[56] concluded that these structures originate from a "carpet-like" dissolution process. The observed structures resemble those observed by Santos et al.,[57] who visualized filipin-induced lesions in planar bilayers by SFM. Compared to the action of phospholipase A_2 on DPPC bilayers as investigated by Nielsen et al.[58] and Grandbois et al.,[59] who found that the enzyme produces small indentations and channels within the lipid membrane preferentially at the border of defects, the effect of melittin without blocking remaining phospholipase activity is much more vivid. It is proposed that the combined action of melittin and phospholipase A_2 results in an ongoing dissolution process in which melittin forms defects, while any remaining phospholipase activity can act at the borders of those defects.

A completely different mechanism was found for the impact of the γ-peptide, a C-terminal capsid protein cleavage product of Flock House Virus (FHV). A Met→Nle variant (Nle = norleucine) of the N-terminal 21 residues of the 44-residue γ-peptide with the amino acid sequence ASNleWERV-KSIIKSS-LAAASNI was synthesized—called γ_1—and the influence on gel-state phospholipid bilayers was investigated by SFM. Janshoff et al.[60] demonstrated that γ_1 exerts a unique effect on neutral gel-phase lipids: Treatment of DPPC bilayers with low mole fractions of γ_1 results in a widespread change in morphology consistent with acyl chain interdigitation of gel-phase phospholipids (Figure 9). The height difference between the two kinds of lipid phases is about (1.5 ± 0.2) nm. Most significantly, increasing the amount of peptide led to an increase in area occupied by the domains of lower height. Treatment of a DPPC bilayer with γ_1 at 0.02 mol% results in line-shaped domains, which comprise 2–6% of the bilayer surface area. At 0.1 mol% peptide concentration the supported membranes are phase-separated with the thinner domains occupying 15–22% of the total area. At 0.5 mol%, the ratio of normal bilayer to compressed area reverses, and the lower domains cover 80–90% of the surface. Above 0.5 mol% peptide, destruction of the bilayers sets in.

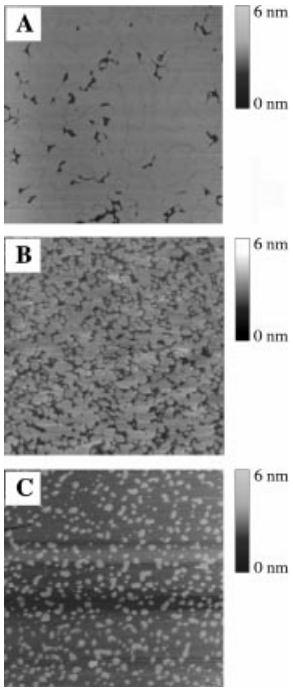

Figure 9. *Formation of compressed domains in a DPPC bilayer on mica by treatment with increasing amounts of γ_1-peptide: A: 0.02 mol%, B: 0.1 mol%, C: 0.5 mol%. The image sizes are $2.5 \times 2.5\ \mu m^2$. (Reprinted with permission from ref. [60]. Copyright 1999 American Chemical Society.)*

Besides these few examples showing the mode of action of membrane-active peptides on solid-supported membranes, a large number of studies involving lipid–peptide monolayers transferred from the air–water interface to a solid support are available. Among them, we selected the example of surfactant-associated proteins B (SP-B) and C (SP-C), two components of the pulmonary lung surfactant, which are responsible for proper lung function and the transition between mono- and multilayers. The pulmonary lung surfactant is a complex mixture of various lipids (content approximately 90%) and four associated protein species forming a thin film at the air–water interface at the inside of the alveoli. The major lipid component is DPPC, which is capable of lowering the surface tension to nearly zero, but is unable to respread fast enough to regenerate the system. Thus, it is assumed that SP-B and SP-C are responsible for surface tension reduction and, more importantly, a fast respreading from surface-associated reservoir structures. SFM has been employed to visualize these reservoirs, proposing a general mechanism of the dynamics of the breathing cycle corroborated by other techniques.

SP-C is composed of 36 amino acids with a molecular weight of 4 kDa and exists solely in a monomeric form adopting a predominantly (approximately 70%) α-helical structure. In most species, SP-C is further modified with two palmitoyl groups covalently linked to the cysteine residues at positions 5 and 6. From SFM, TOF-SIMS analysis, and fluorescence microscopy it is evident that three different structures exist in the plateau region ($54\ mN\,m^{-1}$) of the isotherm of a SP-C, DPPC/DPPG (4:1) mixture.[61–64] Flat patches of pure lipids with virtually no fluorescence emission from protein- or lipid-attached dyes covering about 80% of the overall area and originating from the former liquid condensed (LC) phase are separated from regions showing three dimensional protrusions, which consist of flat bilayer stacks with discrete step heights of 6 nm enriched in SP-C (Figures 10A and D).[65] An intermediate region originating from the former liquid expanded (LE) phase can also be distinguished.

SP-B is a protein with a molecular weight of 18 kDa under nonreducing and 5–8 kDa under reducing conditions. It contains more polar and positively charged residues than SP-C, rendering the protein less hydrophobic. Containing seven cysteines, SP-B is a homodimer, forming three intramolecular and one intermolecular disulfide bridges. Zasadzinski and coworkers[66–68] reported first the influence of SP-B on the phase behavior of lipid films, using fluorescence and Brewster angle microscopy in conjunction with SFM. A thorough SFM study by Krol et al.[69, 70] revealed that in SP-B-containing lipid films, SP-B is located in the LE domains of the lipid matrix, altering the phase behavior and reducing the line tension giving rise to frayed LC domains. At higher surface pressure ($50\ mN\,m^{-1}$), the protein–lipid material forms three-dimensional protein-rich disc-like structures (Figure 10B) accompanied by a change in material properties contrast from rubber-like to a more rigid appearance. It was concluded that SP-B fluidizes lipid monolayers and reduces the domain size of the condensed phase while it stabilizes the film by moving the collapse to higher surface pressure. Owing to the reduction of the LC domain size, SP-B renders the collapse more reversible, since each domain collapses independently, which facilitates respreading of material in the monolayer upon expansion. Remarkably, the protein-rich phase is maintained even at elevated surface pressure. Compared to the SP-C-containing system, protrusions are limited in size and exhibit a globular or disc-like structure of uniform height (8–10 nm). Presumably, the protrusions are bilayer patches mainly composed of peptide and anionic lipids as displayed in Figure 10C. Smaller protrusions permit faster response to changes in surface pressure, therefore rendering the system prepared for a dynamic response.

5. Spatially addressable membranes for creation of rapid screening assays

Artificial solid-supported lipid bilayers may also be used as biological components for biosensor devices providing a variety of advantages over common techniques to immobilize biological molecules. They are inherently highly ordered structures, which efficiently suppress undesired adsorption of molecules and provide an effective barrier for most polar molecules. Moreover, high coverage of the substrate can be achieved by simple techniques, while the deposited membrane accommodates receptor molecules, ionophores, carriers, and transmembrane proteins such as complex ion channels. Attempts have been undertaken to create large arrays of spatially addressable membrane patches to form the basis for a new generation of rapid screening assays and sensor devices based on a highly developed natural environment.[71–75] However, visualization of the micrometer-sized membrane patches was solely performed by fluorescence microscopy. Smaller structures in the nanometer-size regime require new detection techniques with a lateral resolution beyond the resolution of an optical microscope and a detection limit down to a few molecules. Particularly, the combination of high-resolution scanning devices with structured biomolecules on surfaces is advantageous, if the amount of biomaterial is limited or the number of surface reactions is vast. Conceivable applications include the detection of pico- to nanomolar concentrations of proteins such as bacterial toxins binding to cellular receptor molecules.

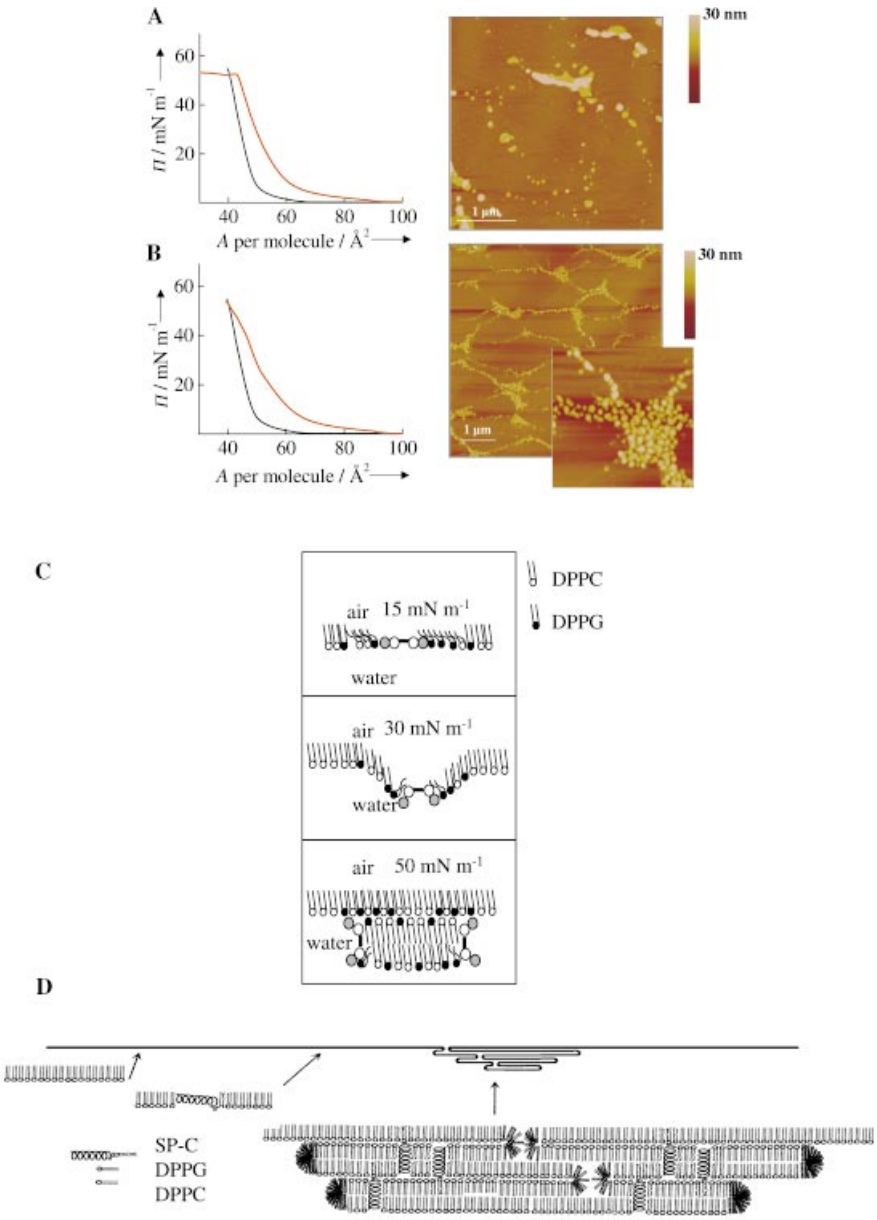

Figure 10. *A: Left: Isotherm of an SP-C-containing monolayer (DPPC/DPPG (4:1), 0.4 mol % SP-C) on a water subphase (red) in comparison to a neat lipid mixture (DPPC/DPPG (4:1), black). Right: SFM image obtained in contact mode under ambient conditions of an SP-C-containing film (DPPC/DPPG (4:1), 0.4 mol % SP-C) transferred at 54 mN m^{-1} onto mica. While SP-B forms disc-like protrusions of one bilayer thickness, SP-C tends to form extended plateaus consisting of stacked bilayers. B: Left: Typical compression isotherms of an SP-B-containing monolayer (DPPC/DPPG (4:1), 0.2 mol % SP-B; red) and a DPPC/DPPG film (4:1; black) without protein at 20 °C on a water subphase. Right: SFM image of an SP-B-containing film (DPPC/DPPG (4:1), 0.2 mol % SP-B) on mica transferred at a surface pressure of around 50 mN m^{-1} from a water subphase at 20 °C. The inset shows a magnification of the disc-like structures. Image size is 1.5 × 1.5 μm^2. C: Possible scenario for the formation of disc-like protrusions of SP-B and negatively charged phospholipids together with an explanation for the mechanistic role of SP-B in a lipid monolayer during compression. D: Proposed model for the observed squeeze out of material supported by SP-C.*[69]

With the aim to achieve small individually addressable membrane structures on solid supports and to utilize SFM to distinguish between adsorbed nonspread vesicles and planar lipid bilayers, Janshoff and Künneke[76] developed a procedure employing a hydrodynamically coupled network of capillaries based on molded polydimethylsiloxane (PDMS) elastomers. Differing in their composition, the membranes should enable one to detect adsorption of proteins and peptides simultaneously by employing SFM. The general technique of using microfluidic networks on glass surfaces, first introduced by Whitesides and co-workers[77, 78] and termed micromolding in capillaries (MIMIC), has been applied by Biebuyck and co-workers[79, 80] to deposit microstructured protein films on surfaces.

The principle of forming membrane patterns by microfluidic networks is outlined in Figure 11 A. Liposome suspensions are applied to one side of the capillaries through which they flow in a laminar fashion and spread onto the glass surface to form a uniform bilayer. After removal of the elastomer, the membrane stripes remain and are stable for days without showing reunion with adjacent membranes. SFM was used to identify the structure and to provide the ultimate proof for the formation of bilayers. Figure 11 B displays an SFM image obtained in contact mode in liquids; it reveals that indeed planar lipid bilayers have been formed on the glass substrate. The average thickness of the DMPC bilayer is (4.2 ± 0.5) nm as deduced from a height analysis (Figure 11 C).

These kinds of patterned lipid membranes varying in their lipid composition and immobilized on a solid support will allow the simultaneous detection of protein binding to one particular membrane stripe with the appropriate lipid mixture by means of SFM in situ.

6. Summary and outlook

SFM of solid-supported lipid bilayers provides insight into dynamic molecular processes and reveals structural details under native conditions not achievable by optical microscopy. Particularly, imaging of 2D crystals of proteins yields structural information with a lateral and vertical resolution that has only been achieved by X-ray crystallography and electron microscopy. Changes in bilayer morphology that are caused by interactions with peptides, membrane-active compounds, or environmental changes can be observed without cumbersome preparation techniques. In conclusion, SFM not only adds to the vast amount of spectroscopic techniques to study membrane – protein interactions, but also opens a new field of research from a material science point

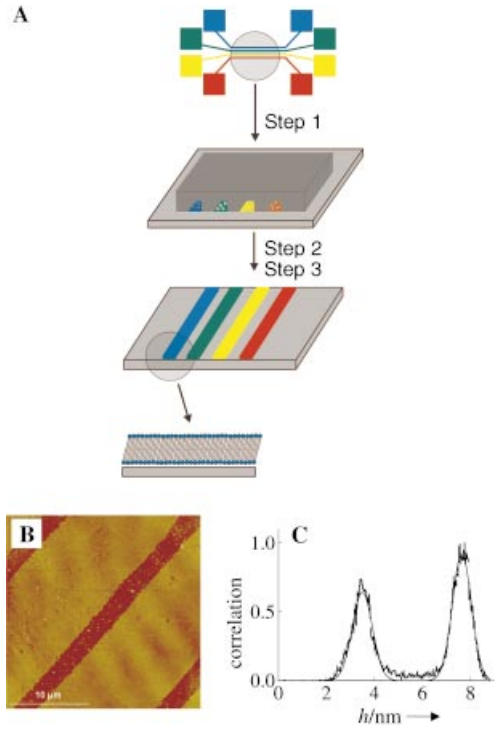

Figure 11. *A: Schematic outline showing the procedure of generating individually addressable patterns of planar lipid bilayers. Step 1: Vesicle suspensions are added to each of the flow-promoting pads on one side. The flow pads on the other side ensure a sufficient flow of liposomes to completely cover the surface with planar lipid bilayers working against depletion; step 2: incubation above the main phase transition of the lipid or lipid mixture; step 3: rinsing with buffer and removal of the PDMS stamp. B: SFM image of planar membranes formed by vesicle spreading along the capillaries. Brighter stripes corresponding to the DMPC bilayers are separated by darker stripes, which correspond to the glass surface. The spacings exhibit a width of approximately 3 μm. The height scale is 20 nm. C: Height analysis of DMPC membrane stripes. Two well-separated height distributions are decomposed by fitting mixed Lorentzian/Gaussian functions to the data shown as solid line. The height difference between the two peaks is 4.2 nm, which corresponds to the height of a DMPC bilayer.*[76]

of view. Not only topographical information may be spatially resolved, but sometimes—even more importantly—viscoelasticity, charge distribution, friction, and binding affinity can be mapped, thus delivering a number of parameters that have been so far unavailable. Future aspects comprise sensor applications utilizing new lithographic techniques to obtain individually addressable membrane compartments combined with the high lateral resolution of scanning probe techniques.

C.S. thanks the Bundesland NRW for a Lise Meitner habilitation fellowship and A.J. thanks the DFG for a habilitation fellowship. The authors would like to thank I. Reviakine and A. Brisson, D. J. Müller, and H. Rinia for providing the excellent SFM figures.

[1] B. Drake, C. B. Prater, A. L. Weisenhorn, S. A. C. Gould, T. R. Albrecht, C. F. Quate, D. S. Cannell, H. G. Hansma, *Science* **1989**, *243*, 1586 – 1589.
[2] I. Reviakine, A. Brisson, *Langmuir* **2000**, *16*, 1806 – 1815.
[3] P. Bassereau, F. Pincet, *Langmuir* **1997**, *13*, 7003 – 7007.
[4] J. Solletti, M. Botreau, F. Sommer, W. Brunat, S. Kasas, T. Duc, M. Celio, *Langmuir* **1996**, *12*, 5379 – 5386.
[5] S. J. Singer, G. L. Nicholson, *Science* **1972**, *175*, 720 – 731.
[6] I. Reviakine, A. Simon, A. Brisson, *Langmuir* **2000**, *16*, 1473 – 1477.
[7] Y. F. Dufrêne, W. R. Barger, J. B. D. Green, G. U. Lee, *Langmuir* **1997**, *13*, 4779 – 4784.
[8] V. Vié, N. Van Mau, E. Lesniewska, J. P. Goudonnet, F. Heitz, C. Le Grimellec, *Langmuir* **1998**, 4574 – 4583.
[9] C. Gliss, H. Clausen-Schaumann, R. Günther, S. Odenbach, O. Randl, T. M. Bayerl, *Biophys. J.* **1998**, *74*, 2443 – 2450.
[10] K. Ekelund, L. Eriksson, E. Sparr, *Biochim. Biophys. Acta* **2000**, *1464*, 1 – 6.
[11] S. W. Hui, R. Viswanathan, J. A. Zasadzinksi, J. N. Israelachvili, *Biophys. J.* **1995**, *68*, 171 – 178.
[12] Z. Shao, J. Yang, *Q. Rev. Biophys.* **1995**, *28*, 195 – 251.
[13] Y. F. Dufrêne, T. Boland, J. W. Schneider, W. R. Barger, G. U. Lee, *Faraday Discuss.* **1998**, *111*, 79 – 94.
[14] J. Schneider, Y. F. Dufrêne, W. R. Barger, Jr., G. U. Lee, *Biophys. J.* **2000**, *79*, 1107 – 1118.
[15] H. Takano, J. R. Kenseth, S. S. Wong, J. C. O'Brian, M. D. Porter, *Chem. Rev.* **1999**, *99*, 2845 – 2890.
[16] The breakthrough force is defined as the force at which the tip breaks through the upper leaflet of the lipid layer and touches the first monolayer.
[17] L. Yang, M. Glaser, *Biochemistry* **1995**, *34*, 1500 – 1506.
[18] M. Ross, C. Steinem, H.-J. Galla, A. Janshoff, *Langmuir* **2001**, *17*, 2437 – 2445.
[19] J. Mou, J. Yang, C. Huang, Z. Shao, *Biochemistry* **1994**, *33*, 9981 – 9985.
[20] Y. Fang, J. Yang, *Biochim. Biophys. Acta* **1997**, *1324*, 309 – 319.
[21] D. M. Czajkowsky, C. Huang, Z. Shao, *Biochemistry* **1995**, *34*, 12501 – 12505.
[22] J. Mou, J. Yang, Z. Shao, *Biochemistry* **1994**, *33*, 4439 – 4443.
[23] H. Mueller, H.-J. Butt, E. Bamberg, *J. Phys. Chem. B* **2000**, *104*, 4552 – 4559.
[24] A. Janshoff, M. Ross, V. Gerke, C. Steinem, *ChemBioChem* **2001**, *2*, 587 – 590.
[25] J. Mollenhauer, *Cell Mol. Life. Sci.* **1997**, *53*, 506 – 507.
[26] M. de la Fuente, V. Parra, *Biochemistry* **1995**, *34*, 10393 – 10399.
[27] L. Oshry, P. Meers, T. Mealy, A. I. Tauber, *Biochim. Biophys. Acta* **1991**, *1066*, 239 – 244.
[28] W. Wang, C. E. Creutz, *Biochemistry* **1994**, *33*, 275 – 282.
[29] V. Gerke, S. E. Moss, *Biochim. Biophys. Acta* **1997**, *1357*, 129 – 154.
[30] I. Reviakine, W. Bergsma-Schutter, A. Brisson, *J. Struct. Biol.* **1998**, *121*, 356 – 361.
[31] I. Reviakine, W. Bergsma-Schutter, C. Mazeres-Dubut, N. Govorukhina, A. Brisson, *J. Struct. Biol.* **2000**, *131*, 234 – 239.
[32] I. Reviakine, W. Bergsma-Schutter, A. N. Morozov, A. Brisson, *Langmuir* **2001**, *17*, 1680 – 1686.
[33] J. Mou, J. Yang, Z. Shao, *J. Mol. Biol.* **1995**, *248*, 507 – 512.
[34] Y. Fang, S. Cheleey, H. Bayley, J. Yang, *Biochemistry* **1997**, *36*, 9518 – 9522.
[35] H.-J. Butt, K. H. Downing, P. K. Hansma, *Biophys. J.* **1990**, *58*, 1473 – 1480.
[36] H.-J. Butt, C. B. Prater, P. K. Hansma, *J. Vac. Sci. Technol. B* **1991**, *9*, 1193 – 1196.
[37] D. J. Müller, F. Schabert, G. Büldt, A. Engel, *Biophys. J.* **1995**, *68*, 1681 – 1686.
[38] D. J. Müller, C.-A. Schoeneberger, G. Büldt, A. Engel, *Biophys. J.* **1996**, *70*, 1796 – 1802.
[39] D. J. Müller, J. B. Heymann, F. Oesterhelt, C. Möller, H. Gaub, G. Büldt, A. Engel, *Biochim. Biophys. Acta* **2000**, *1460*, 27 – 38.
[40] D. J. Müller, D. Fotiadis, A. Engel, *FEBS Lett.* **1998**, *430*, 105 – 111.
[41] A. Engel, C.-A. Schoenenberger, D. J. Müller, *Curr. Opin. Struct. Biol.* **1997**, *7*, 279 – 284.
[42] F. Oesterhelt, D. Oesterhelt, M. Pfeiffer, A. Engel, H. E. Gaub, D. J. Müller, *Science* **2000**, *288*, 143 – 146.
[43] J. H. Hoh, G. E. Sosinsky, J.-P. Revel, P. K. Hansma, *Biophys. J.* **1993**, *65*, 149 – 163.
[44] K. N. Goldie, N. Pante, A. Engel, U. Aebi, *J. Vac. Sci. Technol. B* **1994**, *12*, 1482 – 1485.
[45] S. Scheuring, P. Ringler, M. Borgnia, H. Stahlberg, D. J. Müller, P. Agre, A. Engel, *EMBO J.* **1999**, *18*, 4981 – 4987.
[46] D. J. Müller, D. Fotiadis, S. Scheuring, S. A. Müller, A. Engel, *Biophys. J.* **1999**, *76*, 1101 – 1111.
[47] D. J. Müller, W. Baumeister, A. Engel, *J. Bacteriol.* **1996**, *178*, 3025 – 3030.
[48] D. Fotadis, D. J. Müller, G. Tsiotis, L. Hasler, P. Tittmann, T. Mini, P. Jenö, H. Gross, A. Engel, *J. Mol. Biol.* **1998**, *283*, 83 – 94.

[49] H. Seelert, A. Poetsch, N. A. Dencher, A. Engel, H. Stahlberg, D. J. Müller, *Nature* **2000**, *405*, 418 – 419.
[50] J. Mou, D. Czajkowsky, Z. Shao, *Biochemistry* **1996**, *35*, 3222 – 3226.
[51] H. A. Rinia, R. A. Kik, R. A. Demel, M. M. E. Snel, J. A. Killian, J. P. J. M. Van der Eerden, B. De Kruijff, *Biochemistry* **2000**, *39*, 5852 – 5858.
[52] C. E. Dempsey, *Biochim. Biophys. Acta* **1990**, *1031*, 143 – 161.
[53] Z. Oren, Y. Shai, *Biopolymers* **1998**, *47*, 451 – 463.
[54] Y. Shai, *Biochim. Biophys. Acta* **1999**, *1462*, 55 – 70.
[55] J. A. Kilian, *Biochim. Biophys. Acta* **1998**, *1376*, 401 – 416.
[56] C. Steinem, H.-J. Galla, A. Janshoff, *Phys. Chem. Chem. Phys.* **2000**, *2*, 4580 – 4585.
[57] N. C. Santos, E. Ter-Ovanesyan, J. A. Zasadzinski, M. Prieto, M. A. R. B. Castanho, *Biophys. J.* **1998**, *75*, 1424 – 1429.
[58] L. K. Nielsen, J. Risbo, T. H. Callisen, T. Bjornholm, *Biochim. Biophys. Acta* **1999**, *1420*, 266 – 271.
[59] M. Grandbois, H. Clausen-Schaumann, H. Gaub, *Biophys. J.* **1998**, *74*, 2398 – 2404.
[60] A. Janshoff, D. T. Bong, C. Steinem, J. E. Johnson, M. R. Ghadiri, *Biochemistry* **1999**, *38*, 5328 – 5336.
[61] A. von Nahmen, M. Schenk, M. Sieber, M. Amreim, *Biophys. J.* **1997**, *72*, 463 – 469.
[62] A. von Nahmen, A. Post, H.-J. Galla, M. Sieber, *Eur. Biophys. J.* **1997**, *26*, 359 – 369.
[63] H.-J. Galla, N. Bourdos, A. von Nahmen, M. Amreim, M. Sieber, *Thin Solid Films* **1998**, *327 – 329*, 632 – 635.
[64] M. Amreim, A. von Nahmen, M. Sieber, *Eur. Biophys. J.* **1997**, *26*, 349 – 357.
[65] H.-J. Galla, N. Bourdos, A. von Nahmen, M. Amrein, M. Sieber, *Thin Solid Films* **1998**, *327 – 329*, 632 – 635.
[66] M. M. Lipp, K. Y. C. Lee, J. A. Zasadzinski, A. J. Waring, *Science* **1996**, *273*, 1196 – 1199.
[67] K. Y. C. Lee, M. M. Lipp, J. A. Zasadzinksi, A. J. Waring, *SPIE J.* **1998**, *3273*, 115 – 133.
[68] M. M. Lipp, K. Y. C. Lee, A. J. Waring, J. A. Zasadzinski, *Biophys. J.* **1997**, *72*, 1 – 21.
[69] S. Krol, A. Janshoff, M. Ross, H.-J. Galla, *Phys. Chem. Chem. Phys.* **2000**, *2*, 4586 – 4593.
[70] S. Krol, M. Ross, H.-J. Galla, M. Sieber, S. Künneke, A. Janshoff, *Biophys. J.* **2000**, *79*, 904 – 918.
[71] J. S. Hovis, S. G. Boxer, *Langmuir* **2000**, *16*, 894 – 897.
[72] J. T. Groves, N. Ulman, S. G. Boxer, *Science* **1997**, *275*, 651 – 653.
[73] P. S. Cremer, T. Yang, *J. Am. Chem. Soc.* **1999**, *121*, 8130 – 8131.
[74] P. S. Cremer, J. T. Groves, L. A. Kung, S. G. Boxer, *Langmuir* **1999**, *15*, 3893 – 3896.
[75] L. I. Kung, J. T. Groves, N. Ulman, S. G. Boxer, *Adv. Mater.* **2000**, *12*, 731 – 734.
[76] A. Janshoff, S. Künneke, *Eur. Biophys. J. Biophys. Lett.* **2000**, *29*, 549 – 554.
[77] E. Kim, Y. Xia, G. M. Whitesides, *Nature* **1995**, *376*, 581 – 584.
[78] E. Kim, Y. Xia, G. M. Whitesides, *J. Am. Chem. Soc.* **1996**, *118*, 5722 – 5731.
[79] E. Delamarche, A. Bernard, H. Schmid, A. Bietsch, B. Michel, H. Biebuyck, *J. Am. Chem. Soc.* **1998**, *120*, 500 – 508.
[80] E. Delamarche, A. Bernard, H. Schmid, B. Michel, H. Biebuyck, *Science* **1997**, *276*, 779 – 781.

Received: February 7, 2001 [A 194]